

Chapter 2

Investigating Chromatin Organisation Using Single Molecule Localisation Microscopy

My intention is not to replace one set of general rules by another such set: my intention is, rather, to convince the reader that all methodologies, even the most obvious ones, have their limits.

Paul Karl Feyerabend

2.1 Introduction

In this chapter,¹ I discuss the technical details of single molecule localisation microscopy (SMLM) to investigate spatial and temporal organisation of DNA. The DNA is hierarchically folded at multiple levels to become more compacted and functionally organise itself inside of the nucleus. This spatial arrangement in turn affects the functionality of DNA. Thus one can characterise the organisation of chromatin into three inter-related categories: (1) the basic building blocks, (2) the functional organisation of chromatin and (3) the spatial arrangement of chromatin inside the cell nucleus.

The two classical building blocks: beads-on-a-string and 30 nm chromatin fibre have been extensively studied by EM (Fig. 2.1, first column). Furthermore, one can view functional chromatin domains (Fig. 2.1, second column) as an emerging building block of chromatin, responsible for its basic functions. I estimate these domains to be about 100–400 nm, according to the literature and my own work (see Chap. 3 on interphase chromatin and Prakash et al. 2015; Boettiger et al. 2016; Rao et al. 2014 for more details). These domains are usually the place of chromatin regulation and can display several configurations, depending on their compaction (Fig. 2.1, second column). These compaction states are often associated with different kinds of

¹Parts of this chapter, including figures and captions, are based on the following publications: Szczurek et al. 2014; Żurek-Biesiada et al. 2015, 2016; Hagmann et al. 2014; Best et al. 2014.

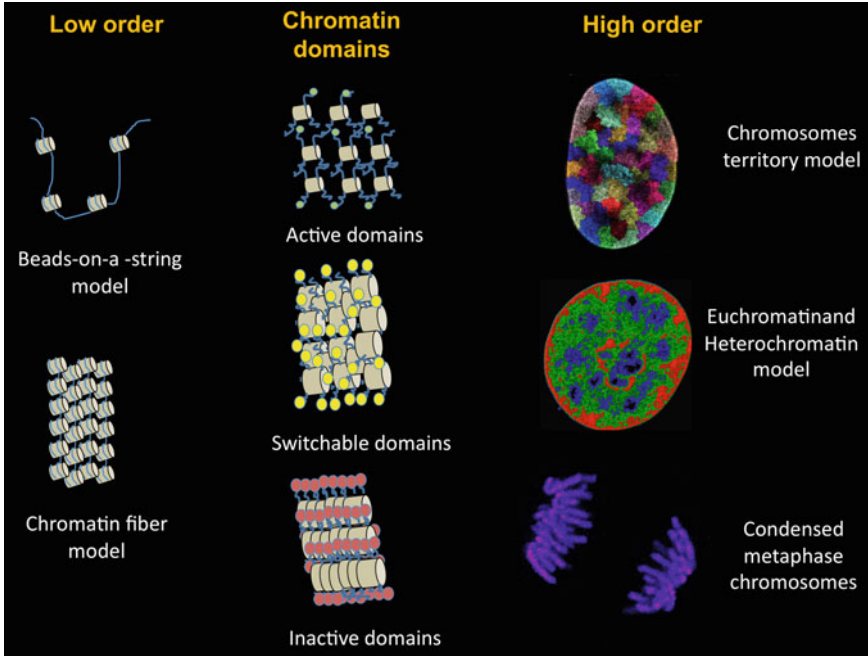


Fig. 2.1 Chromatin spatial organisation: The spatial organisation of chromatin can be studied at three levels: at the lowest orders, which include the beads-on-a-string model and the chromatin fiber, at the level of functional chromatin domains and at high order chromatin patterns. The functional organisation of chromatin domains can be modeled from perspective of various post-translational histone modifications. Depending upon the kind of modification it is enriched with, chromatin can be either highly condensed, in an open conformation or switch between these two extreme forms. The spatial arrangement of chromatin can also be viewed from three points of views: the chromosome territory model of DNA organisation, the bimodal classification condensed and open chromatin in hetero- and eu-chromatin, and finally the highly condensed configuration during metaphase

post-translational histone modifications and can be characterised using information from these modifications (Prakash et al. 2015; Boettiger et al. 2016). Domains can either be highly condensed (usually bearing H3K9me3 modification, a mark associated to the presence of transcriptionally inactive repeated regions) or in an open conformation (mostly at gene promoters and intergenic regions, showing enrichment for H3K4me3, a mark associated to active chromatin). Moreover, chromatin can also be in a state where it switches between these two extreme forms as these domains can also coexist very close to each other (see Chandra et al. 2012; for an overview of the different configurations of chromatin domains using microscopy and genomic data, see Fig. 3.16). Higher orders of chromatin folding, above the chromatin domains, include: the rather outdated bimodal classification of chromatin into condensed and open regions (heterochromatin and euchromatin), the chromosome territory model of DNA organisation (Cremer and Cremer 2001) and finally the highly condensed configuration of the metaphase chromosome (Fig. 2.1, last column).

As chromatin has a highly complex shape, theoretical models are limited to describe its functional structure. Moreover, the organisation of its basic building blocks, the functional and spatial domains, lies between what can be achieved by conventional light microscopy (LM) and electron microscopy (EM). Although EM has provided considerable insights into the structure and organisation of chromatin, as it is not DNA specific, it fails at capturing the underlying nature of the patterns observed. Moreover, sample preparation for EM includes harsh chemical cross-linking and vacuum treatment, which also influence the sample. Light microscopy techniques can be used to study protein and chromatin function in live cells but these methods suffer from much lower resolution than EM.

Super-resolution light microscopy provides an interesting alternative to EM that fills the gap between the resolution achieved by a conventional microscope (Abbe 1873; Rayleigh 1896) and the one required to resolve the individual chromatin domains. The first attempts to improve the resolution used confocal (Cremer and Cremer 1978; Sheppard and Wilson 1981) and multiphoton microscopy (Zipfel et al. 2003), allowing for effective background suppression. The advent of various super-resolution methods (Hell and Wichmann 1994; Heintzmann and Cremer 1999; Gustafsson 2000), in particular, Single Molecule Localisation Microscopy (SMLM) based methods (Betzig et al. 2006; Hess et al. 2006; Rust et al. 2006; Lemmer et al. 2008) have allowed to study objects whose structure lies below the diffraction limit.

2.2 Single-Molecule Localization Microscopy: State-of-the-Art

2.2.1 Principle of SMLM

The underlying principle of most SMLM based methods is to label proteins or DNA/RNA with fluorescent molecules that can reversibly switch between a fluorescent state and a stable dark state. This process of switching between states is called ‘blinking’, and allows for optical isolation of single molecules. Since only a fraction of molecules will switch back to the fluorescent state at a given time, their precise location can be determined. The final accuracy of the position of a molecule depends on the number of detected photons. With a photon count of 10^4 in a single glowing phase, one can achieve a resolution down to a few nanometers (Thompson et al. 2002). In Fig. 2.2, many such molecules are separated by a distance less than $\lambda/(2NA)$ and if all of them are ‘on’ simultaneously then one cannot resolve them. However, if only a few of them are ‘on’ while the neighbouring molecules are in dark state, they can be optically isolated and their precise position can be determined (see Fig. 2.2). Subsequently, if one collects a series of such images where only a few of the molecules are ‘on’ in each image and localise their position, then a final image revealing the structure of the underlying object can be reconstructed (Small and Parthasarathy 2014).

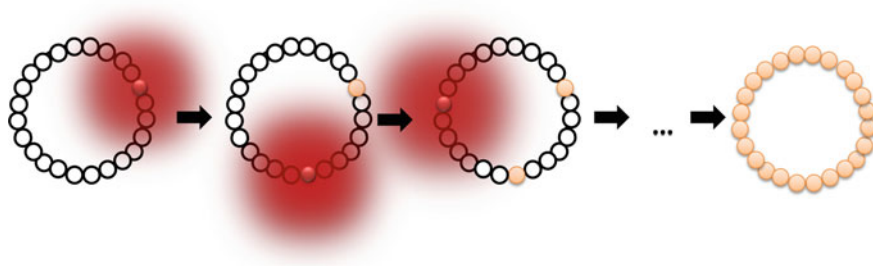


Fig. 2.2 Schematic illustration of the underlying principle of SMLM using a hypothetical object whose building blocks lie below the diffraction limit. This object is made of point sources indicated by *black circles*. Photons emitted by these point sources such as biological molecules or fluorophores are smeared out onto the detector of the imaging system due of the wave nature of light. This distribution of photons is commonly known as the point spread function (PSF) of the imaging system (indicated by the shadow in *red*). PSF has a width of $\lambda/(2NA)$, where λ is the wavelength of the fluorescent light and NA is the numerical aperture. Repeated imaging and localisation of individual fluorophores provides high resolution image of the diffraction limited object if one approximates the position of the molecule as the center of the spot. The photons in the airy disk, which is the central region of the PSF, are thought to have a repartition that follows a Gaussian distribution if the point source emits a sufficient number of photons (Sengupta et al. 2014; Uno et al. 2014)

2.2.2 The Different SMLM Methods: A Historical Perspective

Optical isolation of individual molecules in order to circumvent the resolution limit by acquiring signals at different times has been first theorized in 1985 (Burns et al. 1985), and later included in a comprehensive framework by Eric Betzig of what is now known under name single molecule localisation microscopy (Betzig 1995). Historically, SMLM was first used outside of the chromatin field. Early design by Betzig was successfully applied in 2006 (Betzig et al. 2006) to study cell architecture in a set-up called Photo-activated localization microscopy (PALM). PALM uses two lasers to provoke the blinking of GFP molecules necessary for single molecule microscopy. The first laser (561 nm) is used as the excitation laser while the second laser (405 nm) is used as the activation laser (see (Sengupta et al. 2014) for a review). The structures imaged showed similar level of resolution as electron microscopy, but helped to mark very precisely the position of given proteins on top of the EM image. Set-ups such as STORM (STochastic Optical Recovery Microscopy) use Cy5–Cy3 dye pair as a switch to optically isolate molecules whose separation is below Abbe’s limit. Firstly, all Cy5 molecules are pushed to dark state with a red laser (633 nm) and then a green laser (532 nm) is used to bring a fraction of Cy5 molecules to the florescent state. Though there is no fluorescence from Cy3 itself, a close presence to Cy5 is required for Cy5 to recover from the dark state to a fluorescent emitting state (Rust et al. 2006). dSTORM (direct STORM), a method which extends early observations by (Rust et al. 2006; Lemmer et al. 2008) uses only one laser to push a conventional fluorochrome, for instance Alexa647, between dark and fluorescent

state (Heilemann et al. 2008). Below, I briefly summarize various approaches that led to development of SMLM in its current working form.

- First theoretical approaches: (Burns et al. 1985; Betzig 1995)
- First practical approaches:
 1. Blinking of single molecules (Hirschfeld 1976; Moerner and Kador 1989; Shera et al. 1990; Xie et al. 1994)
 2. Blinking of GFP (Dickson et al. 1997)
 3. Blinking of quantum dots (Lidke et al. 2005)
 4. (fluorescence) Photo-activated localization microscopy (PALM/fPALM, Betzig et al. 2006; Hess et al. 2006)
 5. Stochastic Optical Reconstruction Microscopy (STORM, Rust et al. 2006)
- Methods using standard fluorophores:
 1. Spectral Precision/Position Distance/Determination Microscopy (SPDM, Van Oijen et al. 1998; Lemmer et al. 2008, 2009)
 2. direct Stochastic Optical Reconstruction Microscopy (dSTORM, Heilemann et al. 2008)
 3. Bleaching/blinking assisted localization microscopy (BaLM, Burnette et al. 2011)
- Methods based on binding activation and kinetics: Binding-activated localization microscopy (BALM, Schoen et al. 2011)

Herein, I employed SPDM, the method initiated by (Lemmer et al. 2009) and now known as dSTORM (Heilemann et al. 2008). This method uses a single laser to induce both photoconversion and blinking of a single fluorochrome in one excitation event. This technique was helpful in obtaining a detailed distribution of chromatin, various protein elements and histone modifications, in interphase nuclei (Chap. 3) and during meiosis (Chap. 4). This simple set-up not only enables the analysis of biological samples with the fluorophores used to image DNA molecules in conventional microscopy, but also allows for multi-modal imaging, which can then be used to compare or combine with the results obtained from other microscopic techniques. In this thesis, I discuss various technical aspects of SMLM applied to standard DNA dyes to study chromatin organisation.

2.3 Application of SMLM to Image Chromatin

Chromatin has been a rather recent focus in the field of SMLM. The nano-structure of interphase chromatin was first studied by (Bohn et al. 2010) using SMLM. Statistical methods were combined with SMLM to study the distribution of histone H2B in HeLa and VH7 diploid human fibroblast cells. The main question posed by this study is the possibility of the existence of a recurrent universal chromatin nano-domain and if it can vary across the cell lines and the cell cycle. The author reported



Fig. 2.3 The tao of single molecule microscopy: The two key aspects around which localisation microscopy revolves are localisation precision and signal density. The true representation of the underlying structure is reached when localisation precision and signal density are sufficiently high. Bright fluorophores are required for good localisation precision while for a good signal density, it is required to have only a few of them in each frame which is compensated by acquiring a large number of frames

that chromatin nano-structure is cell type specific and is dependent on the way the chromatin is labelled. A similar conclusion was reached by a recent study (Ricci et al. 2015). Before I probe further into the limitations of these two studies, I would like to discuss two concepts that are central to localisation microscopy: localization precision and signal density.

2.3.1 *The Tao of SMLM*

Two key aspects of SMLM imaging are localisation precision and signal density. Figure 2.3 shows the interplay between these factors. While the bright fluorophores i.e. fluorophores with high photon count are good for localization precision ($\propto \frac{1}{\sqrt{N}}$, where N is the number of photons), it is highly desired to have only a subset of them ‘on’ in each frame (amount of localized events per unit area). To achieve low signal density for each frame, the lifetime of the dark state needs to be significantly longer than the lifetime of the bright state. The overall high signal density (amount of localized events per unit area) is achieved by acquiring a large number of frame so that the theoretical density of the underlying sample is matched.

2.3.2 *Importance of a Good Localization Precision in Order to Improve Resolution*

The resolution of a final reconstructed image in localisation microscopy can be attributed to two separate causes. The first is the fact that like any measurement of a physical quantity, the true value to be measured is only approached at an infinite

number of measurements. Since the photon count of the localization of a fluorophore is limited, the precision with which the fluorophore location can be predicted is limited too. In this analogy a single measurement corresponds to telling which pixel on the light sensitive array was struck by one single photon. Only with the ensemble comprising many photons spread over the adjacent pixels, a highly precise location of the signal can be determined. The precision can be calculated using the Cramér–Rao Lower Bound (Neice 2010; Small and Parthasarathy 2014) and is always above $\lambda/(2NA \cdot \sqrt{N})$, with λ the wavelength of the fluorescent light, NA the numerical aperture (Hagmann et al. 2016) and N the number of photons.

The second cause for resolution reduction results directly from the first (the measurement uncertainty): The fact that the uncertainty of a localized event is isotropic makes it literally impossible to tell in which direction the measured position has to be displaced in order to set it to the true location of the fluorophore (Hagmann et al. 2016). It is important to be aware that the measured position of a fluorophore is not its true position but only the one with the highest probability. The quality of this position estimate is reflected by the localization precision (or uncertainty). In other words, if the same measurement would be carried out several times under the exact same conditions, the acquired locations would be slightly displaced for each measurement. The scale of displacement for every single fluorophore is reflected by its individual localization precision, given by

$$\sigma^2 = \frac{s^2 + a^2/12}{N} + \frac{8\pi s^4 b^2}{a^2 N^2}$$

where s is the width of PSF, N is the number of detected photons, b is the background intensity and a is the size of pixels on the camera.

In Fig. 2.4, I demonstrate that with an increasingly poor localisation precision (from 2 to 100 nm), the point-like-object start to overlap resulting in a blurred image where fine features cannot be resolved. Another point worth noting is that while the first image has the lowest uncertainty (2 nm), the images with 10 and 20 nm uncertainty appear the best. This is due to the fact that higher uncertainty covers for the missing signals by blurring with a bigger radius (see Fig. 2.5)

2.3.3 Importance of High Signal Density to Improve Signal-to-Noise Ratio

One of the key to SMLM is its ability to provide structural information at the highest possible resolution among various super-resolution methods. The structural resolution in localisation microscopy depends upon the localisation precision $\bar{\sigma}_{xy}$ of the individual molecules and the local density of the detected molecules is given by the following formula:

$$\sigma_{xy} = \sqrt{(2.35\bar{\sigma}_{xy})^2 + (2\bar{d}_{NN})^2}$$

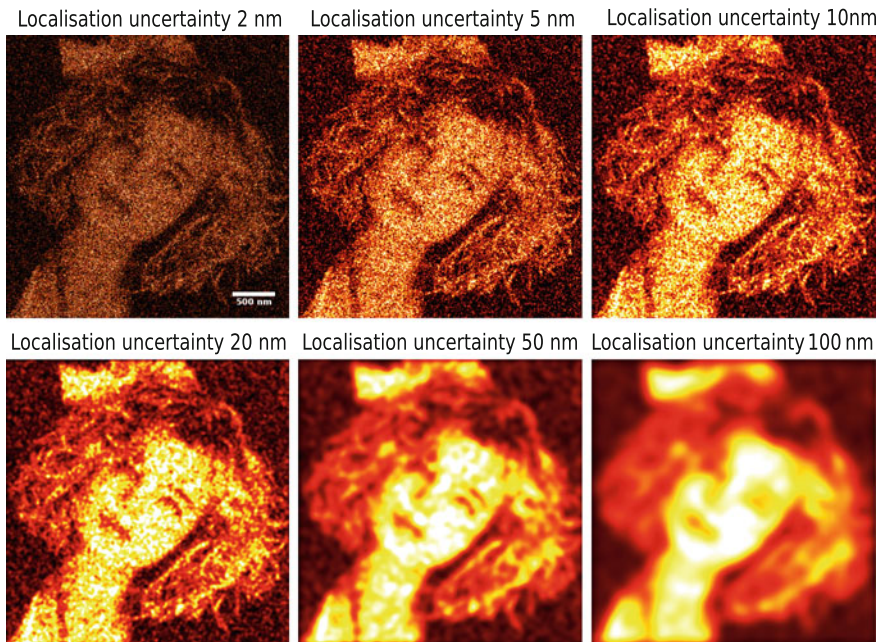


Fig. 2.4 Importance of good localization precision: The measured position of a fluorophore is not its true position but only the one with the highest probability. As the photon budget of a fluorophore is limited, so is the precision with which its position can be localised. In this simulation, I compared the effect of increasing the localisation uncertainty gradually from 2 to 100 nm

$\bar{\sigma}_{xy}$ is the mean lateral localisation accuracy;

\bar{d}_{NN} is the mean distance to the next neighbouring molecules.

The final number of localised signals depends on a number of factors such as labelling efficiency, activation and re-activation frequency and detection efficiency. For example, only a certain percentage of molecules gets labelled and only a subset of these molecules get activated and detected. Furthermore, even a smaller subset of these remaining molecules get reactivated again. This means that only a small subset of the molecules forming the original structure get activated, detected and localised, making it hard to distinguish signals from background. In Fig. 2.5, with 120,000 points one can resolve fine features of Erika's lips (yellow box), while 1000 points are insufficient to draw any satisfactory conclusions. Thus a minimum critical density of signals of at least $\frac{1}{10}$ of the original structure is often required especially if the underlying structure is unknown, a common case for most super-resolution methods. If this is not possible then an intelligent estimate must be made from the prior knowledge based on other studies (for example, EM).

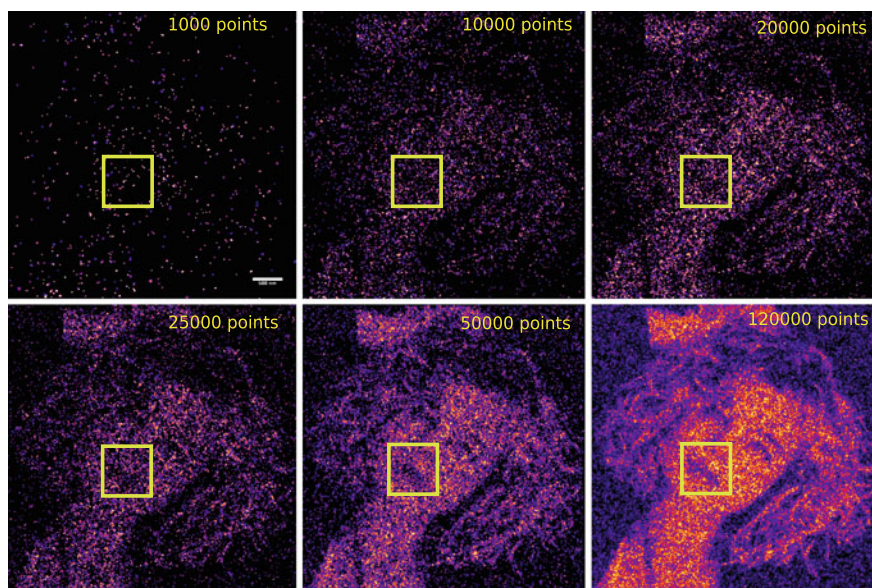


Fig. 2.5 Importance of high signal density: In localisation microscopy, molecules emit fluorescent bursts multiple times before they are bleached (i.e. they stay permanently in dark state), so I use the term ‘signals’ rather than ‘molecules’ here. In all 6 images, the signals were sampled with a localisation uncertainty of 10 nm and the number of signals were gradually increased from 1000 to 120,000 points for a $25 \mu\text{m}^2$ area. A minimum signal density (signal density means the amount of localized events per area) is required to make a first assessment about the underlying structure

2.3.4 Limitations of Previous Approaches to Study Chromatin Organisation

Human genome has roughly 10^9 base pairs and a spherical nucleus ($\frac{4}{3}\pi r^3$) of $10 \mu\text{m}$ radius will have an overall volume of approximately $4000 \mu\text{m}^3$. Since the cells in culture are relatively flat, one can assume that they show an ellipsoid shape ($\frac{4}{3}\pi r^2 a$) with the axial thickness ($a = 2 - 3 \mu\text{m}$) smaller than the lateral radius ($r = 10 \mu\text{m}$). This would bring down the nuclear volume to roughly $1000 \mu\text{m}^3$. Since the observation volume is only a fraction of the total volume, I assume that the final volume of the nuclei imaged would be around $200 \mu\text{m}^3$ with an optical section of $500\text{--}600 \text{ nm}$ axially). So, overall one expects to have around 10^8 putative binding sites/signals in the nuclei. As only a subset of molecules get labelled and are finally detected, the final number of the expected signals is still quite lower. Thus a minimum of $10^7\text{--}10^8$ signals should be detected in order to get a first accurate representation of chromatin distribution inside the cell nucleus (Szcurek et al. 2014).

In one of the previous studies on chromatin organisation, emGFP conjugated histone protein H2B was expressed (Bohn et al. 2010) while in another similar study (Ricci et al. 2015), H2B was immunostained using Alexa Fluor 647. At present,

both of these studies report a labelling density of 100–500 signals per μm^2 and total identified signals in order of 10^4 – 10^5 . At present, both these studies lack sufficient labelling density to make good estimates about the distribution of chromatin inside the cell nucleus.

Here, I focus on improving the method so that the overall signal density and labelling efficiency of DNA molecules is closer to expected binding sites. In the next section, a simple method which uses direct DNA binding dyes and fulfils the above criteria is presented.

2.4 A Method to Reach High Labelling Density of Chromatin with SMLM

Previous studies of chromatin distribution inside of the cell nucleus have relied on a fluorophore conjugated with antibodies targeting chromatin via core histone proteins (Bohn et al. 2010; Ricci et al. 2015) but none has used direct staining of DNA. Recently it was found that DNA minor groove binding dyes, such as Hoechst and DAPI, can undergo UV-induced photo-conversion, to be effectively employed in single molecule localization microscopy (SMLM) with high optical and structural resolution. A proposed mechanism is that these minor groove DNA dyes undergo intra-molecular proton transfer between the phenol group and the bisbenzimidazole nitrogen under UV illumination (Cosa et al. 2001; Carvalho 2010). This UV induced photo-conversion leads to a red shift from the blue emitting form to a green emitting form; a second excitation at a higher wave length will push the fluorochrome to a dark state. This situation eventually induces multiple cycles from dark-state to fluorescent state and back to dark state. Fluorescence of these stochastically blinking molecules is registered by illumination with high intensity 491 nm laser, until bleached (i.e. the molecules are permanently in the dark state). It is worth to note that green-emitting forms of both, Hoechst 33,258 and DAPI occur rather sparsely, facilitating the optical isolation of individual dye molecules bound to DNA (Szcurek et al. 2014). To test if the molecules are really photoconverted, SMLM measurements were performed without any prior illumination with 405 nm line. Subsequently, a significantly lower blinking rate in green-yellow channel was observed, resulting in a poor final reconstruction (data not shown). In the reconstruction from these datasets, fine structures of chromatin could not be resolved. However, with low UV excitation (405 nm), a significant increase in number of molecules in blinking state was observed allowing acquisition of more signals. A 630/90 band pass filter was used to record these signals.

Figure 2.6 shows an optimised adjustment of 405/491 nm laser intensities to study the distribution of chromatin inside a HeLa cell nucleus. Compared with previous studies of histone H2B stably expressed with GFP (Bohn et al. 2010), 50 times more signal density was recorded (124 signals per μm^2 for H2B labelling as compared to 5000 signals per μm^2 here). The nucleus stained with Hoechst (Fig. 2.6a) shows

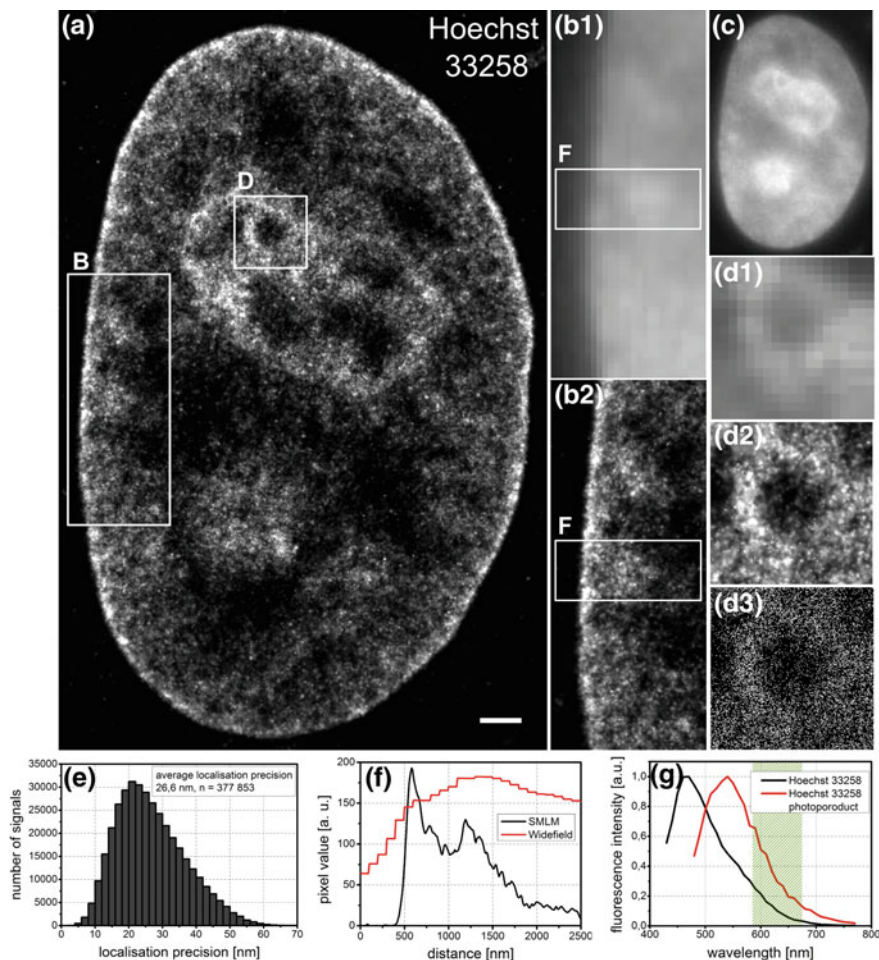


Fig. 2.6 Figure and caption modified from (Szcurek et al. 2014). **a** SMLM image of a HeLa cell nucleus stained with Hoechst 33258. Scale bar: 1 μm . **b1, b2** Widefield and SMLM magnifications of the heterochromatin region highlighted in inset (**b**). **c** Complete nucleus in the widefield mode. **d1–d3** Magnified sections of widefield, SMLM and point representation of nucleolus in (**d**). **e** Histogram of localization precision with average precision around 26.6 nm. **f** Profiles of the heterochromatic region in the boxes of insets B1 and B2, comparing widefield and localisation images. **g** Hoechst 33258 excitation spectrum and the emission spectrum shift of its photoproduct. The green interval is the detection band of the photoproduct

higher density of chromatin around the nucleolus and at the periphery of the nucleus likely associated with hetero-chromatin. Furthermore, a lower density of chromatin is observed towards the interior of the nucleus, in line with previous studies (Cremer et al. 2004; Albiez et al. 2006; Cremer et al. 2015).

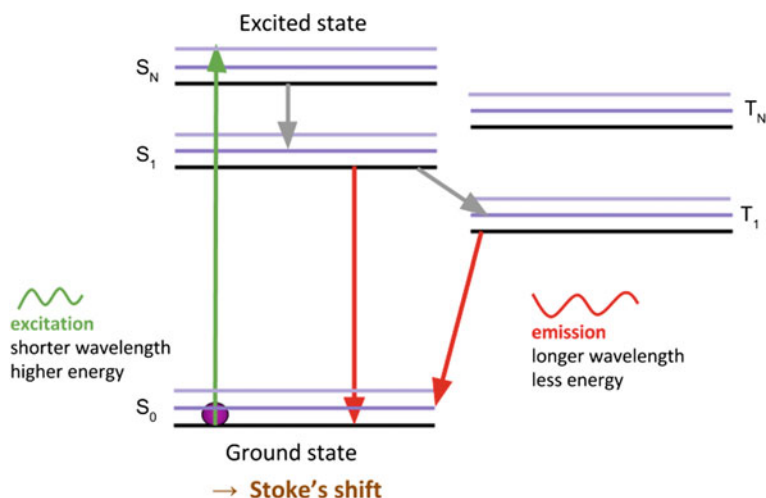


Fig. 2.7 Transitions between excitation states during the fluorescence process. Fluorescence depends on the rapid and lasting rotation between a ground state (electron of low energy) and an excited state (electron of high energy). During relaxation process of the cycle (red arrow), a photon is emitted that produces light. With time, electron can reach other intermediate states called triplets (T_1 and T_N here) that can lead to the deteriorative oxidation of the fluorochrome, resulting in bleaching

2.4.1 Theory of DNA Dye Fluorescence

Molecules with multiple aromatic cycles which bind the small groove of DNA, such as DAPI, can potentially emit fluorescence. In solution, the structure of the molecules shows a high flexibility, but while interacting with DNA, they become stabilized and display a planar structure, which enhances the degrees of freedom of circulating electrons across aromatic cycles or other features of the molecule. This situation has both effects of increasing the probability of capturing incident photons, as the surface of the molecule increases, and the probability to observe an electron hit by a photon, as an electron occupies more space at a given time (Biancardi et al. 2013 and Fig. 2.7).

2.4.2 Adapting Study of DNA Dyes Fluorescence to SMLM

Application of blinking properties of DNA dyes to SMLM stems in the photoconversion of individual molecules followed by their excitation to the dark state, a concept pioneered by Betzig using GFP (Dickson et al. 1997; Betzig et al. 2006). The method has two steps:

1. Optimization of photo-conversion, to ensure that the pattern of photo-converted molecules is optimal to generate blinking patterns.
2. Optimization of buffers, to push a higher number of fluorochrome molecules to photo-conversion and delay bleaching of molecules.

2.4.3 Optimization of the Photoconversion Process

This step optimizes the amount of molecules photo-converted to obtain high density of signals. The signals are optimally spread in time so that one does not acquire too many signals in a single frame, otherwise one gets unresolved points and poor resolution. To achieve this, the intensity and the timing of photo-conversion, via a 405 nm wave length excitation pushing DAPI or Hoechst to a green form, has to be calibrated properly. If photo-conversion is absent, the final number of detected signals is low and the final reconstruction is impaired (Fig. 2.8).

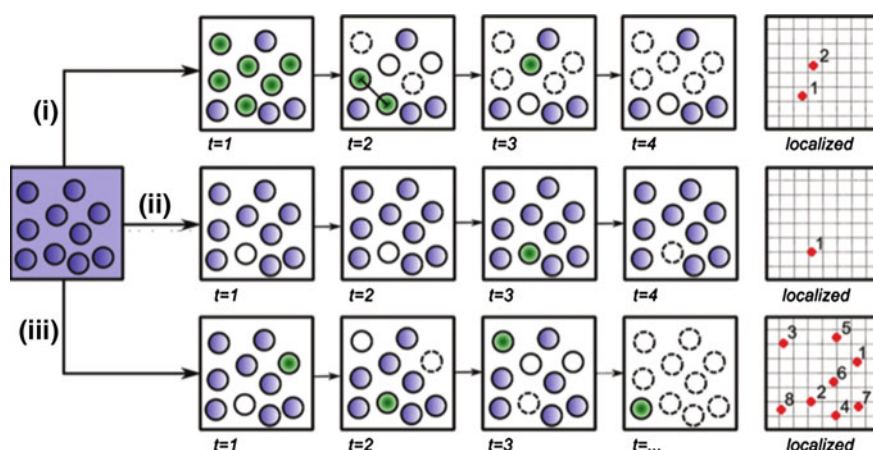


Fig. 2.8 Optimization of the photoconversion process to obtain good resolution and signal density. Obtaining a good blinking pattern is dependent on mild photoconversion. Excessive photoconversion (i) leads to large number of molecules photoconverted and will not be detected along the different frames, preventing optical isolation of single molecules (poor resolution, average density of points). (ii) Insufficient photoconversion separates molecules properly, but does not generate enough signals to reconstruct the initial object (high resolution, low density of points). (iii) An optimized set-up will generate homogenous photoconversion of molecules in time, resulting in both good separation of signals across time points and a high final signal density, allowing a more accurate reconstruction of the initial object (high resolution, high density of points). Figure modified from (Szcurek et al. 2014)

2.4.4 Optimization of the Buffer Conditions

A strong element in the optimization of the protocol to employ conventional DNA dyes for imaging of DNA molecules is the usage of an effective buffer. Usage of mixes with high concentrations of glycerol seems to be the best option according to recent benchmarks (Żurek-Biesiada et al. 2016). Beside preserving the nuclear morphology, glycerol prevents the generation of reactive oxygen species (ROS) from the reaction between the fluorochrome and surrounding dioxide molecules. This reaction releases oxygen atoms with a free radical, which are very hostile for biological molecules such as DNA (Bernas et al. 2004). Glycerol can compete with the fluorochrome for interaction with the free radical, preserving the fluorochrome from degradation (Hussels and Brecht 2011). This results in a better photoconversion than if the DNA dye was subjected to more Brownian movements (Biancardi et al. 2013).

2.4.5 Multicolor Imaging with DNA

To analyse the spatial arrangement of different nuclear proteins with respect to DNA, optimization of various conventional dyes was studied along with DNA dyes and summarised in Fig. 2.9. It is further hoped that the dyes presented in Fig. 2.9 will be optimised to allow the visualization of more fluorochromes within one experiment. This will further enable the analysis of spatial arrangements of various other components of the nucleus in conjunction with chromatin at the level of individual nuclei.

2.4.6 A Summary of Various Approaches Used to Study DNA with SMLM

The strategies to study chromatin inside the cell nucleus can be divided into two broad categories: (1) Direct labelling of DNA and (2) indirect labelling of DNA. Below I provide a brief summary on various approaches that have been used to study chromatin/DNA with SMLM which is pictorially summarised in Fig. 2.10.

• Direct Staining Methods

1. **YOYO-1** is a DNA intercalating dye binding between the two strands of DNA. YOYO-1 and PicoGreen (which binds to the major groove) were previously used to study the organisation of bacterial chromosomes with SMLM (Schoen et al. 2011). The authors called this method binding-activated localization microscopy (BALM) because both YOYO-1 and PicoGreen bind directly to the DNA and these molecules only get activated when bound to the DNA. This is a good way to improve both labelling efficiency and localisation accuracy as DNA binding

Fluorophores:		Quality of blinking in buffer composed of GOX/CAT/Glycerol/10% glucose	Excitation Wavelengths required [nm]:
DNA dyes	DAPI*	++	405 + 491
	Hoechst 33258*	+++	405 + 491
	Hoechst 33342*	+++	405 + 491
	Vybrant dyecycle Violet*	+++	491
Other	Alexa 488	++	491
	Atto 488	+++	491
	Alexa 546	+	561
	Alexa 555 ^S	++	561
	Alexa 568 ^S	+++	561
	Alexa 647*	++++	647 + 491
	Atto 655	+++	647
	Alexa 660*	++	647 + 561
	Alexa 680*	++	671 + (405 / 491 / 561)

Fig. 2.9 Comparison of various DNA dyes and other fluorescent probes. Quality of blinking as well as suitable wave lengths are indicated. Asterisks indicate that blue shift needs only a low excitation to happen. Dollars indicate that dual color imaging can be performed without correction of chromatic shift. Table is reprinted from (Żurek-Biesiada et al. 2016)

increases specificity and is closer to the actual target than antibodies are. These dyes have been shown to work for lambda phage DNA stretches but not for structures which have much higher chromatin density, for example, mammalian cell nuclei. A report of a successful application of YOYO-1/SMLM to staining of eukaryotic nuclei will be presented in Chap. 3.

2. **Hoechst, DAPI and Vybrant Violet (VV).** Conceptually this is similar to the binding-activated localization microscopy (BALM). DNA minor groove binding dyes such as DAPI or Hoechst do not 'blink' in their standard form. However, with low dose of 405 nm laser, a small proportion of molecules can be photo-converted to green form and start to blink, a property applicable to localisation microscopy. It is proposed that upon UV illumination, these dyes, which either undergo protonation or become photoconverted from blue to green emitting form, might also be driven by hydrogen peroxide (Piterburg et al. 2012). It

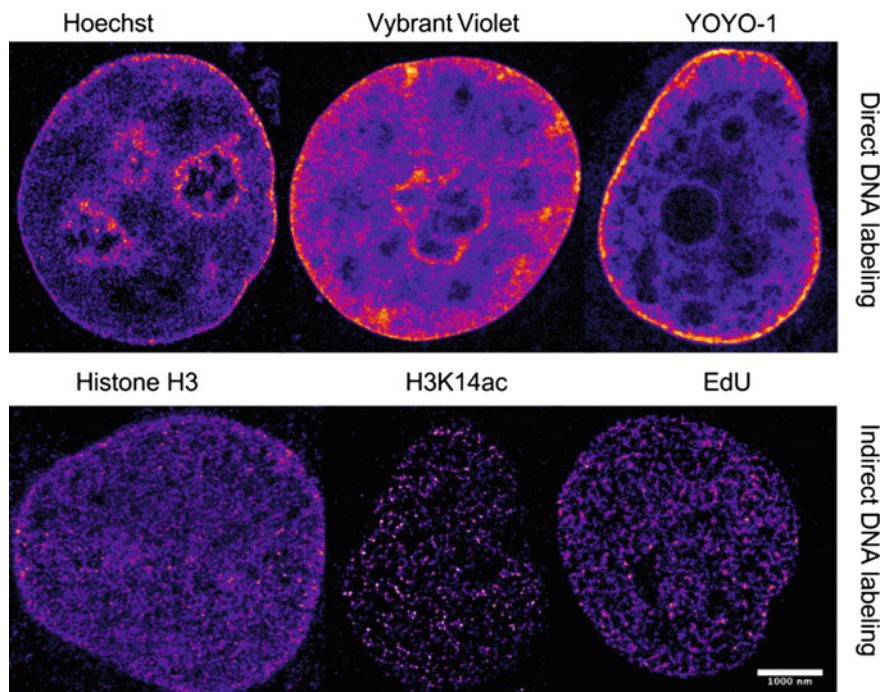


Fig. 2.10 Comparison of direct and indirect DNA labelling. Top block shows various DNA minor groove binding dyes that can be used to study the distribution of the chromatin inside the cell nucleus. Bottom block shows examples of indirect methods (immunostaining and EdU incorporation) to study the distribution of chromatin inside the cell nucleus

must be noted that only one wavelength (491 nm) is required for activation and excitation in the case of VV.

3. **Propidium Iodide or DRAQ5** are non-cyanine intercalators that also bind directly to DNA. However, their applicability in superresolution microscopy has yet to be demonstrated.

• Indirect Staining Methods

1. **EdU incorporation:** Zessin et al. 2012 were the first to describe a high resolution structure of DNA using precursor incorporation. The authors used EdU (5-ethynyl-2'-deoxyuridine) labelling using click chemistry to image nascent DNA produced during DNA replication. Click-chemistry is a copper-induced covalent binding between an alkyne group of EdU and an azide present in the chemically modified fluorophore (Grammel and Hang 2013). This method has two main advantages. Firstly, it is highly specific. The alkyne-azide bond is not commonly found in any biological system and the method is very specific and sensitive. Because of this specificity, the method produces almost no

background. Secondly, it is less harmful compared to other popular precursors such as BrdU (Baskin et al. 2007; Grammel and Hang 2013).

2. **Core histone proteins:** Bohn et al. 2010 studied chromatin organisation inside the cell nucleus by fusing one of the core histone proteins (H2B) with GFP. In this study, H2B was either stably integrated (H2B-GFP) or over-expressed (H2B-emGFP) in the HeLa cells. In other studies, either immuno-labelling against core histone proteins (H3, H2B) was used or cells were transfected with H2B-mEos2 or H2B-PAmCherry for live cell imaging (Ricci et al. 2015).
3. **Histone modifications:** To study functional chromatin and its compartmentalization, histone modifications were recently used to describe chromatin organisation (Prakash et al. 2015; Boettiger et al. 2016). These two studies were based on antibody labelling of specific histone modifications. The main problem with such labelling methods is the huge size of primary and secondary antibody (molecular weight around 150–200 kDa) and the linker length i.e. the distance between the true position of the molecule and the position where the signal is detected, which can be in the order of 7.5 nm for a primary antibody and in the order of 15 nm for a secondary antibody.
- **Sequence specific imaging of DNA:** It is often desired to study specific loci of gene or other DNA sequences instead of the entire chromatin. This specific staining can be performed using Fluorescence *In Situ* Hybridization (FISH) (Weiland et al. 2011), oligonucleotide probes (Cremer and Cremer 2001; Müller et al. 2010) or via genome editing techniques such as transcription activator-like effectors (TALE), (Miyazari et al. 2013; Thanisch et al. 2013) CRISPR/Cas9 techniques (Anton et al. 2014; Chen et al. 2013; Wood et al. 2011; Hsu et al. 2014; Doudna and Charpentier 2014) or SNAP-tag fusion proteins (Klein et al. 2011).

Figure 2.10 compares the overall staining of the cell nucleus with direct and indirect staining. One can observe that direct staining of DNA leads to a more continuous distribution of chromatin as compared to indirect staining, where the distribution seems to be in a speckle-like patterns (see also Bohn et al. 2010; Ricci et al. 2015 for recent examples of low labelling density). This happens because in specific staining only the functional compartments, usually associated to specific histone modifications, are revealed. For example, H3K14ac is associated with active transcription and hence only sites where chromatin is in a more open conformation fluoresce. Similarly, in EdU incorporation (Fig. 2.10, bottom right) only the freshly replicated sites from S-phase are detected (see Chap. 3 for more examples of these two cases).

2.5 SMLM Microscope Design and Imaging Pipeline

The basic set-up for SMLM imaging is very similar to the configuration of a wide-field microscope. In the following sections, various aspects of the SMLM such as sample preparation, data acquisition, data reconstruction, data visualisation and data analysis are discussed.

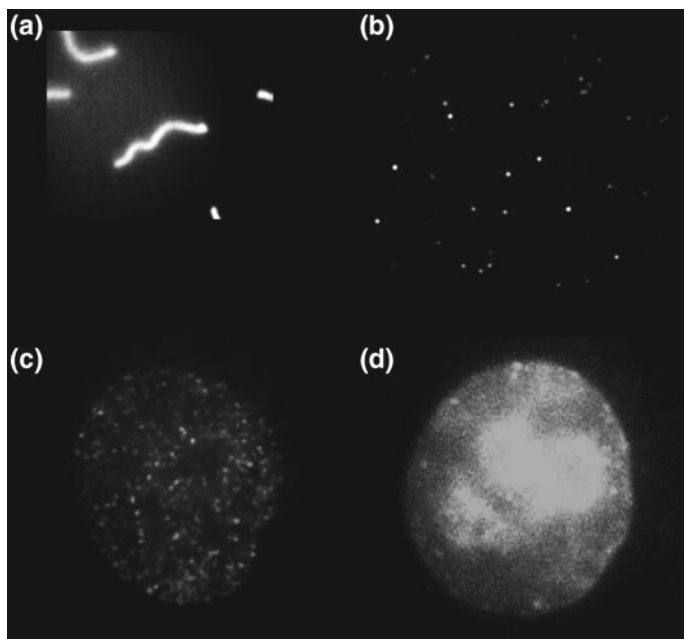


Fig. 2.11 Different kinds of background in a SMLM measurement: **a** No blinking. All signals are considered as background. **b** No background, a typical PALM set-up in TIRF mode with only blinking molecules. **c** Uniform background. **d** Highly spatial and temporal non-uniform background

2.5.1 Sample Preparation for SMLM

A good SMLM sample follows three criteria. (1) The nano-structure is preserved. (2) A high number of fluorophores bind to the target. (3) Non-specific labelling and background are minimised (Bates et al. 2013). For preservation of nanostructure, optimised fixation protocols from EM can be used. Optimization of buffer is key and usage of reactive oxygen species competitors which prevent fluorochrome from degradation can help. Background/non-specific signal can severely decrease the quality of a superresolution reconstruction (Betzig et al. 2006). A comparison of different background scenarios is shown in Fig. 2.11. Use of thin samples in addition to an appropriate imaging buffer can help to minimize the background.

2.5.2 Imaging Medium

Usage of photo-convertible DNA dyes (Hoechst, DAPI and VV) requires certain components to be present in the 'switching buffer'. In particular, the switching buffer should contain 0.5 mg/ml Glucose oxidase, 0.04 mg/ml Catalase, 0.1 g/ml glucose in

PBS. The use of MEA, one of main components of the STORM/dSTORM imaging buffer diminishes the rate of switching in the case of DNA dyes. The switching buffer facilitates the switching of the steady fraction of spontaneously blinking molecule in each frame. The switching buffer is the same as the oxygen scavenger system in STORM/dSTORM, which mainly reduces photo-bleaching fluorescent dyes. More details on imaging medium can be found in (Szcurek et al. 2014; Żurek-Biesiada et al. 2015, 2016).

2.6 Data Acquisition for SMLM

For imaging DNA with photoconvertible DNA dyes, several important aspects have to be considered. Firstly, low power 405 nm illumination in conjunction with a 491 nm laser should be used to increase the number of detected molecules. Similar ideas were previously described in (Heilemann et al. 2008) for photoswitchable fluorescent dyes. However, these dyes have no affinity for DNA. The SMLM measurements were performed with a vertical/upright microscope set-up (see Fig. 2.12). The set-up has four laser sources with excitation wavelengths at 405, 491, 561 and 647 nm and can be dissected into 3 modules described below.

1. **The illumination module:** The laser beam enters the microscope via mirrors (M) and dichroic mirrors (DM) [M1–M4, DM1–DM4], a collimator arrangement (5x expansion of beam diameter) and neutral density filters (if required). This collimator is made up of two achromates with focal lengths of 30 and 150 mm which expand the beams by a factor of 5 to get an homogeneous illumination of the sample.

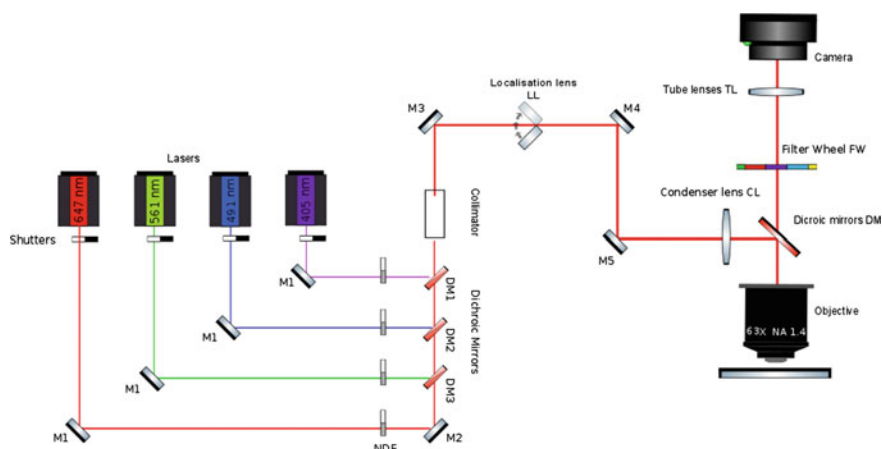


Fig. 2.12 A schematic of the SMLM microscope. For description of optical parts, refer to the text

2. **The localisation module:** To achieve the high laser intensity for the localization mode, a lens [LL] is inserted in the optical pathway, leading to a smaller illuminated area of higher intensity in the object region of interest. The beam is focused by this lens into the back focal plane of an oil immersion objective lens (63x, NA = 1.4). The sample is actuated by a piezoelectrical stage [PS] for focusing.
3. **The detection module:** The emitted fluorescent light goes through the DM and is focused by a tube lens [TL] (1.0x, $f = 200$ mm) onto the CCD chip of a highly sensitive 12 bit black-and-white camera. A set of appropriate blocking filters is mounted in a filter wheel [FW] in front of the camera chip.

Before acquiring data, certain parameters have to be optimised. For example, bleaching gradient, blinking and their relation to integration time must be studied prior to the measurement and the final number of acquisition frames should be chosen accordingly. One should try to optimise the integration time of the camera as this determines signal-to-noise ratio and eventually the background of the sample. Acquisition of wide-field images before and after measurement helps to compare the structure of the sample with the final reconstruction. Illumination of the sample should be homogeneous. Furthermore, to fasten the acquisition time and save disk space, the sample area can be restricted to a region of interest.

2.7 Data Reconstruction for SMLM

Figure 2.13 presents various steps required to reconstruct a highly resolved image from single molecule coordinates. The operations can be characterized at various levels which are described below.

- **Stack level:** A high number of frames with each frame containing only a few optically isolated molecule must be generated. This data stack can be used to analyse the position of the fluorophore across multiple frames and characterise the fluorophore. Furthermore, a background map for each frame must be calculated and subtracted to get the difference image. This step can be really critical depending on the type of background in the sample (refer Fig. 2.13.)
- **Frame level:** Local maxima in each frame are determined and the corresponding regions-of-interest (ROI) are extracted.
- **ROI level:** Each fluorophore is localised and an estimate about the localisation precision for each molecule based on the parameters of the model function should be calculated. An estimation about the number of photons per molecule is then calculated, an important parameter to study the characteristics of the fluorophores used in the experiments.
- **Error corrections:** Signal from a particular fluorophore occurs more than once during an acquisition and subsequent frames. Removal of signals in multiple consecutive frames is important, so that the same fluorophore is not counted twice. If the sample moved significantly during acquisition, the drift in the sample must be corrected, a common procedure for measurements of long duration. Finally, the events that do not fulfil other quality criteria are removed.

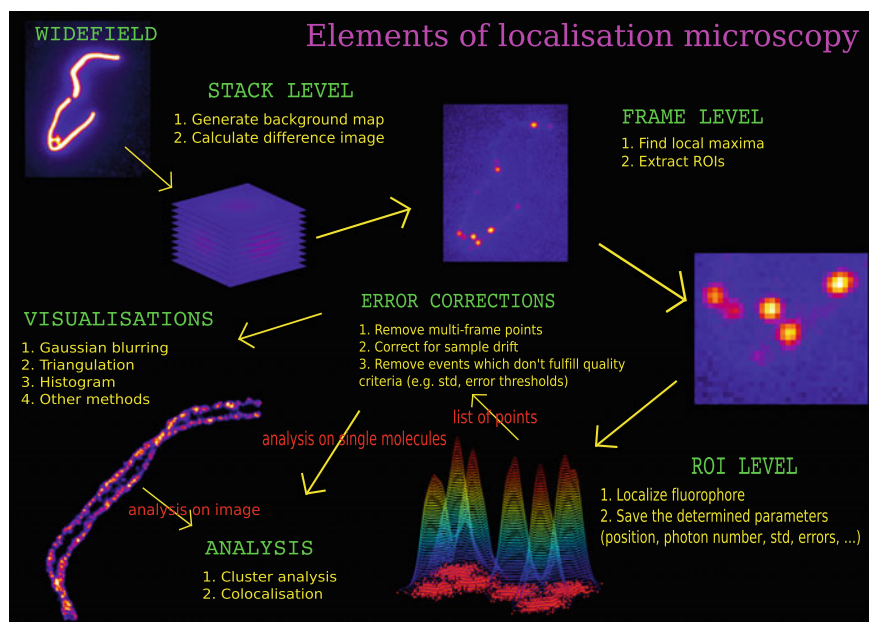


Fig. 2.13 SMLM data reconstruction and analysis flowchart. ROI: Region of interest. See text for details

- **Visualisation:** The position of the single molecules should then be visualised to get a nanoscale representation of the biological object. Visualisation methods include for example, Gaussian blurring, triangulation and histogram methods. A visualisation method is selected based on the labelling density and/or the prior knowledge about the underlying structure from other methods such as EM.
- **Analysis:** Finally, different kinds of analysis such as co-localisation, cluster analysis, nearest neighbour, density analysis can be performed on either high resolution images or coordinates of single molecules.

2.7.1 Spot Finding for SMLM

Algorithms used to precisely identify the locations of fluorophores can be broadly classified into two categories, fitting based and non-fitting based (usually Centroid) methods. While iterative fitting-based methods can usually provide fitted parameters equal or close to the maximum likelihood estimate, *ad hoc* centroid based methods are usually very fast. However, any localisation method will struggle if the underlying model poorly represents the observed data e.g. in case of a high background level, presence of out of focus signals or noise, etc. A particular challenge for the exact fluorophore determination is posed by both spatially and temporally

fluctuating background intensities arising from out-of-focus blinking fluorophores. This can happen if the structure is not *per se* 2-dimensional (e.g. PALM using TIRF illumination, see Fig. 2.11). In the following sections, I discuss these two broad categories of localisation methods.

Fitting Based Methods

Photons emitted by point sources are smeared out onto the detector of the imaging system due to the wave nature of light. This smear or blur is described by the point spread function (PSF) of the imaging system. The intensity distribution of a photon at the detector follows an Airy function but for practical purposes is approximated with a Gaussian function. The overall model function consists in a 2D Gaussian describing the PSF, a function describing the background level and one more term to describe the noise. The model function is represented by:

$$I(x, y) = \frac{A}{2\pi\sigma_x\sigma_y} \exp \left[-\frac{1}{2} \left(\frac{(x - x_0)^2}{\sigma_x^2} + \frac{(y - y_0)^2}{\sigma_y^2} \right) \right] + B + N$$

where x, y are the coordinates of the point emitters, σ_x, σ_y are the width of the distribution, A the peak intensity value of the distribution, $2\pi\sigma_x\sigma_y$ the normalisation factor, x_0, y_0 the coordinates of the real center of the distribution, B the background level and N the noise parameter.

The next task is to optimise the parameter values in order to minimise the error between the signal and the model. The optimisation can be done on all the parameters or just on the coordinates of the emitter positions. Two common methods to optimise the parameters are the least squares method (LSM) and the maximum likelihood estimation (MLE). The principle behind both methods is the same. In LSM, the difference between the signal and model on each pixel is calculated and the error is then squared and added. Based on the error sum, new parameter estimates are made and the sum of the squared errors is calculated again to check if the updated parameter values reduce the error. This process is iterated until the least summed errors are obtained.

In the MLE, the overall process is the same except that detailed information about the experimental conditions such as knowledge about the PSF, noise, background is required. Similarly to LSM, the difference between the signal and the model is calculated and statistics of noise are then used to predict how likely the difference between the model and the signal is. The parameters are tuned to maximise the likelihood of the data. Cramer–Rao Lower Bound (CRLB) states that MLE makes more precise estimates compared to LSM or other parameter optimisation methods (Small and Stahlheber 2014; Small and Parthasarathy 2014).

Non-fitting Based Methods

The fitting methods are often computationally intensive and difficult to handle when the sample is inhomogeneous. Another approach is to find the coordinates of the

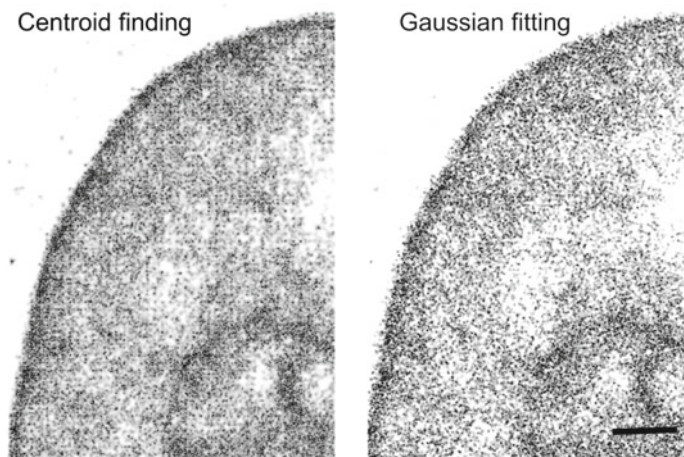


Fig. 2.14 Various reconstruction algorithms for SMLM: Fitting (Gaussian) and non-fitting (centroid) reconstruction algorithms are compared. While non-fitting algorithms are fast, fitting algorithms are more accurate. The grid-like patterns are frequently observed when high density data are reconstructed with centroid method (see text for more details and Best et al. 2014). Scale bar: 1 μm

centroid of the fluorescent spot or in the case of isotropic emitters to take advantage of their radially symmetric shape to estimate the coordinates. When the background is non-uniform and so localisation density is high, due to the additive nature of background noise at regions with high localisation density, the coordinate estimates are biased towards the center of the ROI, often resulting in a grid like patterns (Fig. 2.14 and Best et al. 2014). Various filtering methods should be used to reduce the background intensity and improve the coordinate estimation. For more details on various algorithms estimating the emitter coordinates, please refer to (Small and Stahlheber 2014; Small and Parthasarathy 2014; Chenouard et al. 2014).

2.7.2 Drift Correction Algorithms for SMLM

The correct position determination of fluorescent molecules is crucial for the interpretation of the localisation microscopy data, e.g. to understand the biological structure investigated. The position of fluorophores is highly sensitive to environmental disturbances (e.g. acoustic vibrations) and to mechanical instabilities of the microscope hardware (e.g. thermal expansion, stage drift). These disturbances can cause distortion in the recorded image, significantly affecting the achieved localisation accuracy, especially when it is in the order of tens of nano-meter or better. Previously, on line drift correction methods have been described, which estimate and correct the drift experienced during recording of the experiments. Predicting the drift for future frames is a hard task, as behaviour of vibrations can not be predicted. This can easily be done after measurement.

With colleagues, I developed a drift correction strategy based solely on already acquired data without any fiducial markers (Hagmann et al. 2014). It was found that in some SMLM set-ups (PALM, STORM), most of the biological samples exhibit enough permanent (photostable) structure that can be used at several time points to gain information about the sample. This information was used to correct the lateral drift based on the underlying structure visible in a raw image sequence (averaged over 10 subsequent frames for one sample image), to then calculate the auto-correlation between sample images. Then two (for x and y) eighth order Fourier series were fitted to the acquired data in order to obtain the drift vectors. Figure 2.15a, b shows HeLa cell nucleus stained with Hoechst 33258 photo-product before and after drift correction. The long acquisition times resulted in considerable mechanical drift of the stage. In

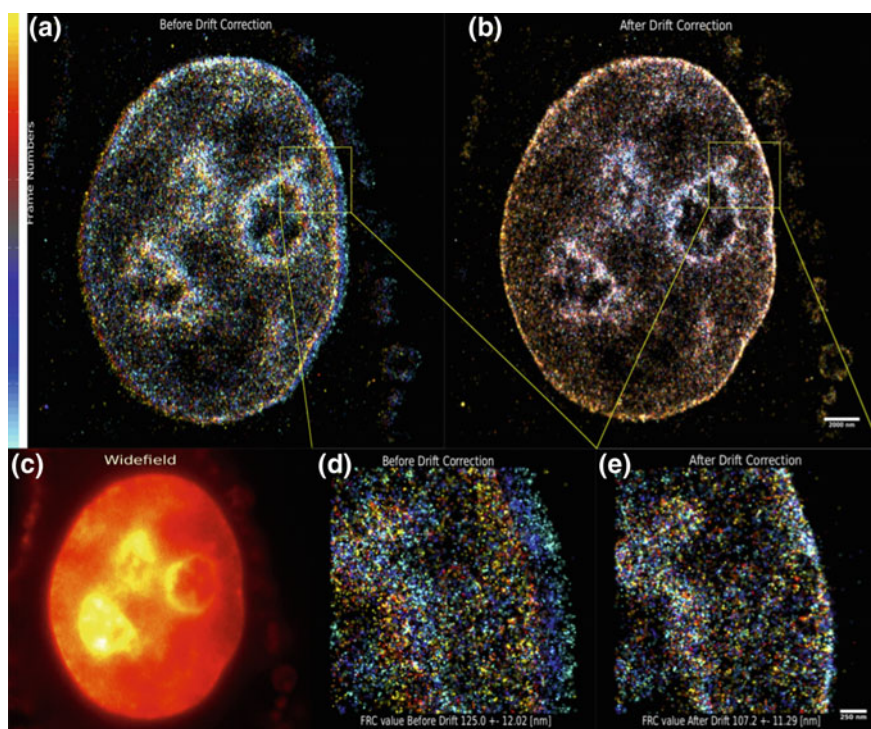


Fig. 2.15 Structured based drift correction strategies for localisation microscopy: Some variants of localisation microscopy exhibit enough permanent (photostable) structure that can be used to correct the lateral drift based on the underlying structure visible in a raw image sequence. HeLa cell nucleus stained with Hoechst 33258 photoproduct before (a) and after drift correction (b) are shown. c Widefield image of the same nucleus. Due to long measurements, the initial drift was found to be in the order of 500–1000 nm. d–e After application of structured based drift correction algorithm drift improved to less than 20 nm, well within the localisation precision. The magnified sections (D and E) show significant improvement in resolution (computed using FRC method (Nieuwenhuizen et al. 2013)). The resolution before drift correction was 125 nm and improved down to 107 nm after (Hagmann et al. 2014)

the Fig. 2.15, the frames of the data stack are color coded to demonstrate the drift in the sample. The initial frames are coloured blue, while the final frames range from yellow to white. The sample can be seen to drift from top right to bottom left. For the SMLM microscope used for the measurement, the drift was in order of 100–1000 nm (Fig. 2.16a) and was determined by image phase correlation. A polynomial or Fourier series (equation below) was fitted through the data, from which the dislocation of every event was subtracted.

$$y = a_0 + \sum_{i=1}^n a_i \cos(iwx) + b_i \sin(iwx)$$

where a_0 is the intercept term in the data (associated with $i = 0$ cosine term), w the frequency of the signal and n the number of harmonics (8 in our case).

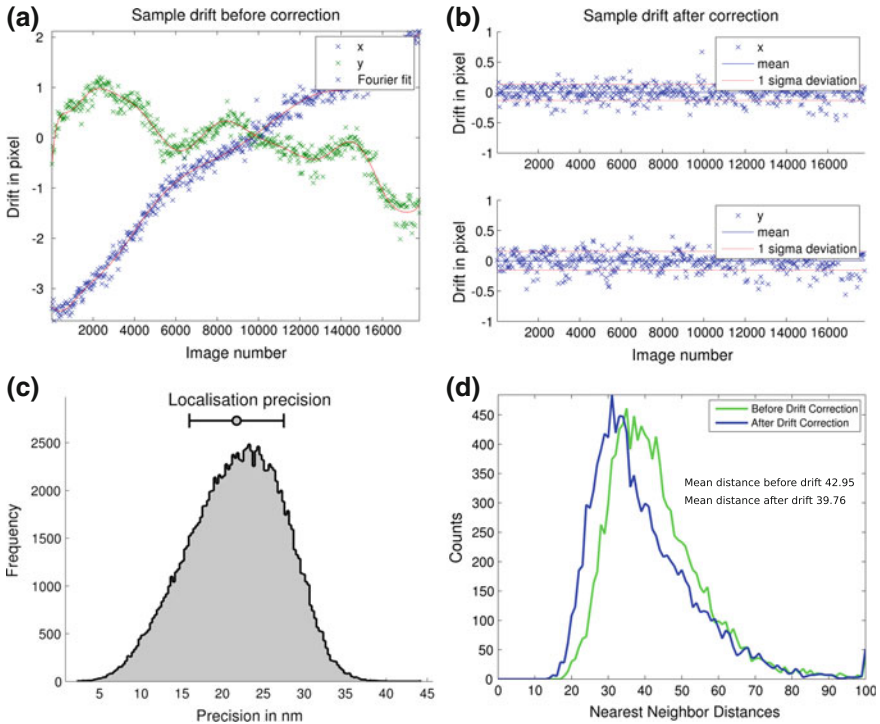


Fig. 2.16 Quantification of sample drift. **a** The drift along x axis was less than 200 nm, however the drift along y axis was in order of 500 nm. **b** After application of structured based drift correction algorithm, the overall drift in both x and y directions was less than 20 nm, well within the localisation precision (**c**). **d** shows the nearest neighbor distances before and after drift correction. The mean nearest neighbour distance before drift was 42 nm while it improved to 39 nm after correction

In the present case of a cell nucleus with high background, the data were corrected to a final drift under 20 nm (Fig. 2.16b), which was reasonable given the high localisation precision (average 25 nm, Fig. 2.16c). Furthermore, the resolution computed based on Fourier ring correlation (Nieuwenhuizen et al. 2013) showed a significant enhancement in resolution before (125 ± 12 nm) and after (107 ± 11 nm) drift correction. The drift correction also resulted in significant improvement of neighbour distances. The mean nearest neighbour distances before and after drift correction were approximately 42.95 nm and 39.76 nm in the zoomed sections of the cell nucleus (Fig. 2.15d, e and Fig. 2.16d).

Overall, the drift correction resulted in increased local density of chromatin at the nuclear periphery, which is in accordance with nuclear architecture. It is believed that with appropriate drift correction strategies, one can observe true structural features which are often accompanied with a decrease in nearest neighbour distances. Structure based drift correction demonstrates high background and that the underlying structure of datasets can be used to correct drift. Using this approach, one can successfully correct the localisation microscopy data down to a final drift under 5 nm. The results are comparable to fiducial markers based strategies. Moreover, the resolution of the final reconstructions is substantially enhanced and the natural limit of localisation precision is achieved.

2.7.3 Data Visualisation for SMLM

While most imaging modalities generate an image, SMLM provides coordinates single molecules in addition to the image common to the other superresolution methods (STED and SIM). Previously, scatter-gram of point positions (Hess et al. 2006; Van Oijen et al. 1998), 2D histogram of point positions (Heilemann et al. 2008; Lemmer et al. 2008; Fölling et al. 2008; Egner et al. 2007), localisation precision based Gaussian blurring (Betzig et al. 2006; Rust et al. 2006), nearest neighbour blurring of molecule positions (Kaufmann et al. 2012) and triangulation of localisations (Baddeley et al. 2010) have been the most popular visualisation methods.

In Fig. 2.17, localisation precision based Gaussian blurring, triangulation and nearest neighbour blurring of individual molecule are compared. When enough number of nearest neighbour molecules are taken into consideration (20 in the present case), the underlying structure becomes increasingly visible. This happens because blurring locations with a Gaussian is not the best choice when the labelling density is low. In such a case the pointillist appearance of the emitters resurfaces in the final image. Moreover, there is a resolution loss factor of $\sqrt{2}$ as stated in (Baddeley et al. 2010). However, nearest neighbour blurring is helpful at revealing structures especially if the sample suffers from a low density of points. Moreover, the points that are not part of a structure are suppressed. Finally, the visualisation method is chosen based on the labelling density and the characteristics of the structure to visualise (1D, 2D or 3D).

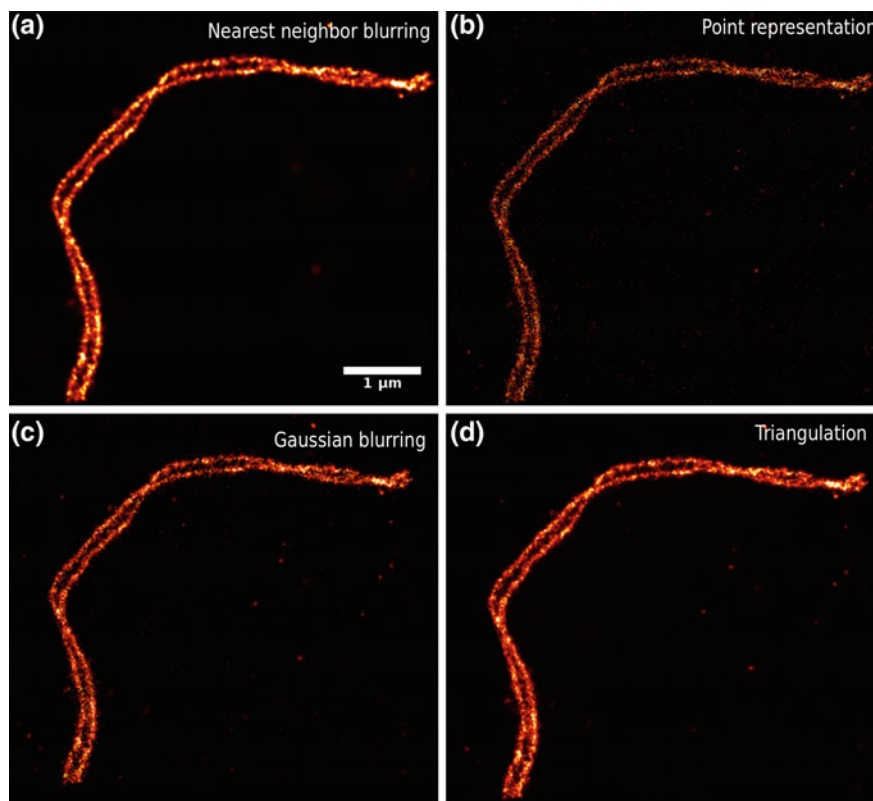


Fig. 2.17 Comparison of various visualisation algorithms: Comparison of Gaussian blurring based localisation precision, triangulation and nearest neighbour blurring of individual molecules is shown. When enough nearest neighbour points are taken into account, the underlying structures can be better observed. Nearest neighbour blurring can help to bring out the underlying structure in images lacking proper labelling density. Moreover, the points that are not part of the structure are suppressed. Figure and caption modified from (Prakash et al. 2015)

2.7.4 Data Analysis for SMLM

Advent of various super-resolution microscopy methods have brought to light various diffraction limited biological objects, revealing periodic patterns (Prakash et al. 2015; Fröh et al. 2015; Xu et al. 2013) under better resolution. The analysis of periodicity in these studies (Fröh et al. 2015; Xu et al. 2013) was based on the intensity information of the images. In addition to pixel intensity information, SMLM provides information about the single molecule coordinates which can also be used for autocorrelation and periodicity analysis.

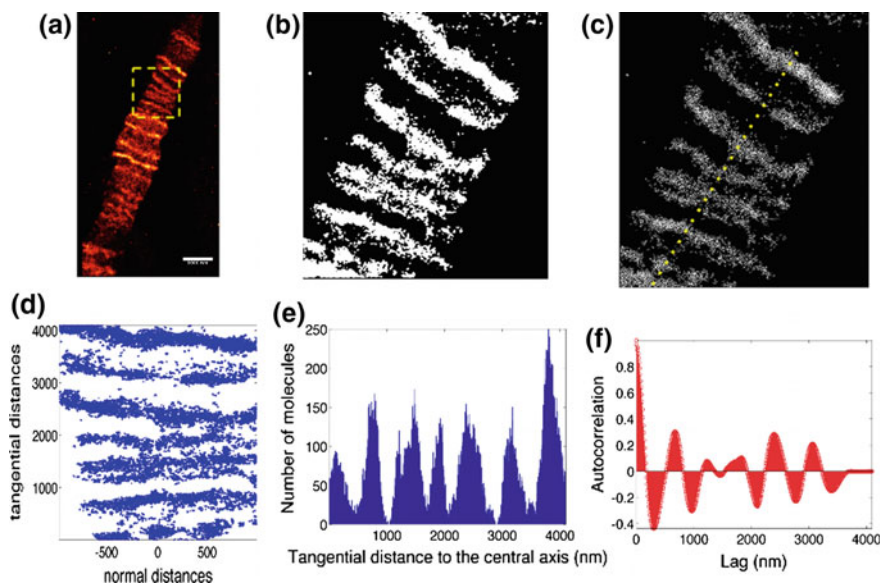


Fig. 2.18 Various steps involved in single molecule autocorrelation. **a** Firstly, each molecule is blurred using the value of the mean distance to 20 nearest neighbour points. **b** Secondly, a binary mask is generated based on the nearest neighbor image and **c** only the signals within the binary mask are considered for further analysis. **d** Each molecule position is then translated to Cartesian coordinates for the ease of analysis. **e** A histogram of the tangential and normal positions is generated. **f** Finally the bins of the histogram are auto-correlated to estimate the periodicity

Single Molecule Autocorrelation

For single molecule autocorrelation, each localisation was blurred with 20 nearest neighbours and a binary mask was generated (see Fig. 2.18) using a global threshold described elsewhere (Prakash et al. 2015; Jianzhuang et al. 1991). The single molecules within this binary mask were extracted for further analysis. This resulted in keeping only the molecules which belong to the structure or the clusters considered. For the autocorrelation analysis, a line was fitted manually to pass through the center of the object. The coordinates were then translated and rotated to get a more linear orientation. Finally, the autocorrelation values were calculated on the histogram of the tangential distances along the central axis. The algorithm is described in detail in (Prakash et al. 2015).

2.8 Some Further Considerations for Localisation Microscopy

There are a number of artefacts that can arise due to sample preparation mainly due to fixation conditions, permeabilization conditions, antibody concentration and the type of buffer used. These are described in detail in (Whelan and Bell 2015). Here, I discuss three more kinds of artefacts that can arise from the way microscope is set up and the coordinates of single molecules are estimated post-acquisition.

2.8.1 *Artefacts in Localisation Microscopy*

Figure 2.19 shows negative of wide-field and localisation image of a HL-1 cell nucleus stained with Hoechst. Due to the non-homogeneous illumination of the sample (Fig. 2.19a), the lower left of the cell nucleus is more illuminated than the upper right part of the nucleus. This leads to a non-uniform detection of molecules across the sample. For example, the chromatin density at the nuclear periphery (the upper right part of the image in (Fig. 2.19a, b) is higher than the lower left part of the image. The same pattern of density can also be observed around the nucleolus (black arrows). Another factor that can lead to a non-homogeneous illumination of the sample is the Gaussian profile of the excitation beam. In such a case, the central regions are more illuminated than the regions toward the periphery of the nucleus.

Another type of artefact can arise due to the data reconstruction when there is a high number of signals in each frame (Fig. 2.19c). The high density leads to the overlap of the signal resulting in a grid-like patterns. If the centroid fitting algorithm or center-of-intensity (COI) is used to localise the signals then the signal is biased toward the center of the pixel resulting in grid-like patterns (see Sect. 2.7.1). However, no grid-like pattern is observed with Gaussian fitting, which is more accurate but slower when compared to centroid fitting. One solution to solve this problem is to make sure only few signals blink in each frame so signals do not overlap and can be optically isolated. Then one has to take a high number of frames to get a high density super-resolved image. This can be achieved by initial reversible photo-bleaching of the sample before acquisition and waiting until the uniform blinking of the signals is achieved.

A third type of artefact is experienced when biological objects under study are poorly labelled. The pattern which are obvious in wide-field image are missed in the high resolution images. Such an example can be seen in Fig. 2.20. Pol II is known to form barrel-like elongated shapes in polytene chromosomes (Zhimulëv 1996) which are apparent in wide-field image (Fig. 2.20a, inset a1). However, SMLM imaging does not reconstruct these apparent patterns of Pol II (Fig. 2.20b), following the well-known alternation patterns of dense and light regions of polytene chromosomes (Zhimulëv 1996). Pol II-rich regions are enriched for genes, and correspond to the dense regions of electron microscopy images, while Pol II-poor regions

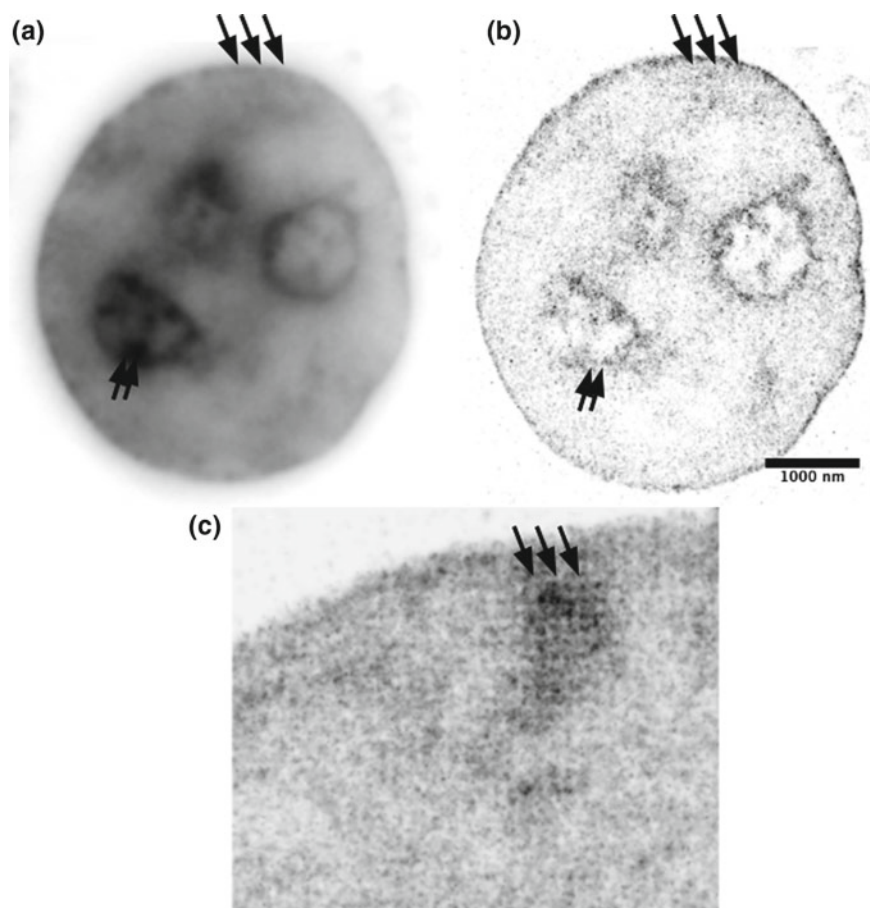


Fig. 2.19 Artifacts in localisation microscopy: **a** Negative of a widefield image of HL-1 cell nucleus stained with Hoechst. **b** Negative of high resolution reconstruction of the same cell. Dense chromatin blob is observed around the nucleolus (black arrows inside the nucleus) in **(a)** but is missing in **(b)**. Moreover, no dense chromatin is observed at the nuclear periphery in **(a)** but is present in the high resolution reconstruction in **(b)**. This is usually due to non-homogenous illumination of the sample. One factor that can generate non-homogenous illumination is the Gaussian profile of the high intensity excitation beam that causes the central region in widefield mode to be illuminated more than the peripheral regions. **c** A section of the nucleus showing a grid-like pattern. Such patterns usually arise in high density single molecule reconstructions when the Center-Of-Intensity (COI) algorithm is used. COI biases the localisation towards the center of the CCD camera pixel, giving rise to such grid-like patterns

correspond to light regions, deprived of genes. This example shows a major pitfall of super-resolution imaging, particularly prominent when the underlying structure is unknown and poor or insufficient labelling of the biological object might lead to a wrong interpretation of the data. This also reflects the importance of a good in-depth

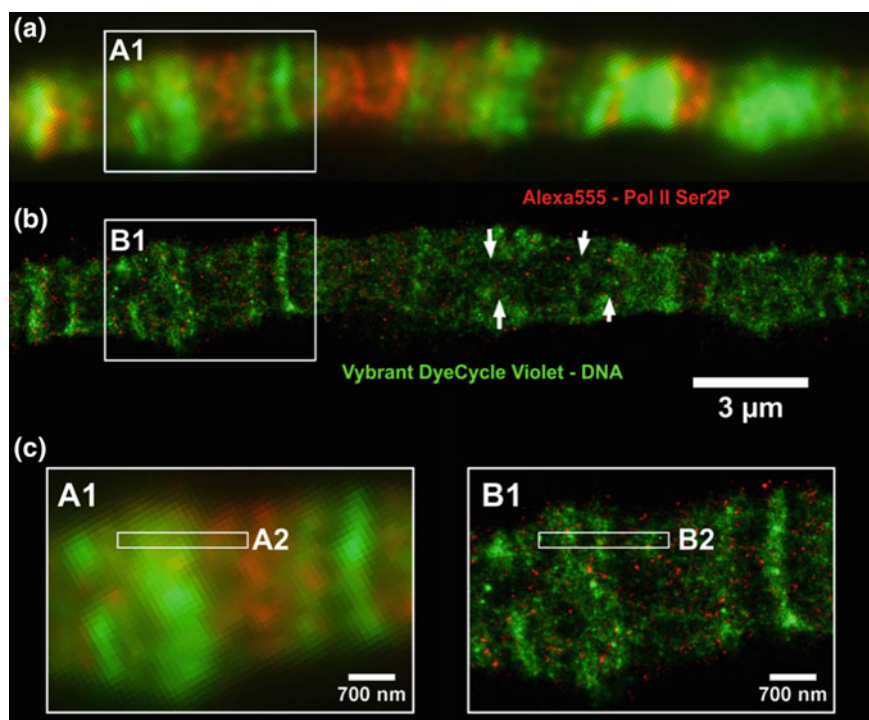


Fig. 2.20 Dual color SMLM image of *Drosophila* polytene chromosome stained with VV (green) and Pol II Ser2P-Alexa Fluor 555 (red). **a** Widefield image of a fragment of a polytene chromosome. **b** SMLM images of the fragment as in (a). Arrows indicate regions of loose chromatin inside the polytene chromosome. **c** Enlarged fragment of the images shown in A and B, embracing dense heterochromatic and lower density eu-chromatic regions of DNA. Figure and caption modified from (Żurek-Biesiada et al. 2015)

literature survey about the biological object and the importance of blurring when the labelling density is limited.

2.8.2 *Difference Between Localisation Precision and Accuracy*

The terms localisation precision and accuracy are often used interchangeably. Localisation precision is the exactness with which the position of a signal can be predicted, which can be slightly off the true position of the molecule. This distance between the true position of a molecule and the detected signal is the localisation accuracy. Figure 2.21a, shows a detected signal slightly off from the true position of the molecule. As the signals are not spread, the localisation precision will be good but the

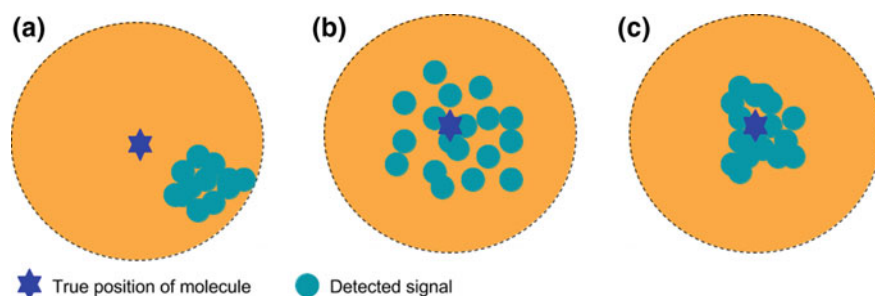


Fig. 2.21 Localisation precision Vs localisation accuracy: **a** Good localisation precision but poor localisation accuracy. **b** Good localisation accuracy but poor localisation precision. **c** Good localisation accuracy and localisation precision. The true position of a fluorophore is indicated by a *blue star* while turquoise blobs indicate the detected signal

localisation accuracy will be poor. In the second case (Fig. 2.21b) the detected signals are spread over a large region resulting in a poor localisation precision but an increased localisation accuracy as the detected signals are close to the true position of the molecule. In the third case (Fig. 2.21c), localisation accuracy and precision are both high, a typical case for Hoechst and DAPI which directly bind to DNA (high localisation accuracy) and display a high photon count (high localisation precision).

2.9 Summary

Single Molecule Localisation Microscopy (SMLM) is one of the major emerging tools for the analysis of biological structures at approximately 10nm spatial resolution. The procedure relies on sequential detection of (a subset of) individual fluorophores. For dense regions (fluorophores with significant overlap), a compromise between labelling density and the photoswitching behaviour of fluorophores is needed to optically isolate molecules in each acquired frame. The last 10 years have seen a significant progress in fluorescence imaging with the development of new fluorescent probes and the discovery of new properties of existing fluorochromes (Szcurek et al. 2014; Żurek-Biesiada et al. 2015), making them applicable for super-resolution imaging.

Until recently, description of chromatin was limited to immunostaining of histone proteins, which does not provide enough labelling efficiency and density for chromatin imaging (Bohn et al. 2010; Ricci et al. 2015). Nevertheless, usage of conventional dyes dramatically increases the amount of signals recorded, opening avenues for the description of chromatin architecture at all levels of magnification. This is the matter of the next two chapters; Chap. 3 discusses many structural features of chromatin found in interphase, while Chap. 4 presents recent results regarding the chromatin architecture of the pachytene chromosome. Both these aspects of chro-

matin organisation grandly benefit from the developments presented in the current chapter. In this chapter, I discussed the theory and concepts of SMLM, as well as sample preparation, hardware implementation, data reconstruction, visualisation and quantifications. I closed the chapter with a note about localisation accuracy, precision, resolution and some of other technical pitfalls.

With more efficient fluorophores (i.e. with higher photon counts), highly sensitive camera, high NA objective lenses, an even higher spatial resolution can be expected in the future. A particular important challenge is live cell imaging, which requires both high spatial and temporal resolution though efforts in this direction are already being made (Biteen et al. 2008; Shroff et al. 2008). Single particle tracking is another area where photo-switchable fluorescent probes will facilitate tracking of high-density particle in live cells (Manley et al. 2008). Finally, I hope that together with SIM, SMLM can be broadly applied to chromatin biology and other areas of cell biology to provide insights into the nuclear architecture at nanoscale.

References

- Abbe E (1873) Beiträge zur Theorie des Mikroskops und der mikroskopischen Wahrnehmung. *Archiv für Mikroskopische Anatomie* 9:413–420. doi:[10.1007/BF02956173](https://doi.org/10.1007/BF02956173)
- Albiez H, Cremer M, Tiberi C, Vecchio L, Schermelleh L, Dittrich S, Küpper K, Joffe B, Thormeyer T, von Hase J et al (2006) Chromatin domains and the interchromatin compartment form structurally defined and functionally interacting nuclear networks. *Chromosom Res* 14(7):707–733
- Anton T, Bultmann S, Leonhardt H, Markaki Y (2014) Visualization of specific dna sequences in living mouse embryonic stem cells with a programmable fluorescent crispr/cas system. *Nucleus* 5(2):163–172
- Baddeley D, Cannell MB, Soeller C (2010) Visualization of localization microscopy data. *Microsc Microanal* 16(01):64–72
- Baskin JM, Prescher JA, Laughlin ST, Agard NJ, Chang PV, Miller IA, Lo A, Codelli JA, Bertozzi CR (2007) Copper-free click chemistry for dynamic in vivo imaging. *Proc Natl Acad Sci* 104(43):16793–16797
- Bates M, Jones SA, Zhuang X (2013) Stochastic optical reconstruction microscopy (storm): a method for superresolution fluorescence imaging. *Cold Spring Harbor Protoc* 2013(6):pdb-top075143
- Bernas T, Zarebski M, Cook RR, Dobrucki JW (2004) Minimizing photobleaching during confocal microscopy of fluorescent probes bound to chromatin: role of anoxia and photon flux. *J Microsc* 215(3):281–296
- Best G, Prakash K, Hagmann M, Cremer C, Birk U (2014) Identify and localise: algorithms for single molecule localisation microscopy. In: Hozák P (ed) 18th international microscopy congress, number ISBN 978-80-260-6720-7
- Betzig E (1995) Proposed method for molecular optical imaging. *Opt Lett* 20(3):237–239
- Betzig E, Patterson GH, Sougrat R, Wolf Lindwasser O, Olenych S, Bonifacino JS, Davidson MW, Lippincott-Schwartz J, Hess HF (2006) Imaging intracellular fluorescent proteins at nanometer resolution. *Science* 313(5793):1642–1645
- Biancardi A, Biver T, Secco F, Mennucci B (2013) An investigation of the photophysical properties of minor groove bound and intercalated dapi through quantum-mechanical and spectroscopic tools. *Phys Chem Chem Phys* 15(13):4596–4603

- Biteen JS, Thompson MA, Tselentis NK, Bowman GR, Shapiro L, Moerner WE (2008) Super-resolution imaging in live *caulobacter crescentus* cells using photoswitchable eyfp. *Nature Methods* 5(11):947–949
- Boettiger AN, Bintu B, Moffitt JR, Wang S, Beliveau BJ, Fudenberg G, Imakaev M, Mirny LA, Wu C-T, Zhuang X (2016) Super-resolution imaging reveals distinct chromatin folding for different epigenetic states. *Nature* 529(7586):418–422
- Bohn M, Diesinger P, Kaufmann R, Weiland Y, Müller P, Gunkel M, Von Ketteler A, Lemmer P, Hausmann M, Heermann DW et al (2010) Localization microscopy reveals expression-dependent parameters of chromatin nanostructure. *Biophys J* 99(5):1358–1367
- Brooks Shera E, Seitzinger NK, Davis LM, Keller RA, Soper SA (1990) Detection of single fluorescent molecules. *Chem Phys Lett* 174(6):553–557
- Burnette DT, Sengupta P, Dai Y, Lippincott-Schwartz J, Kachar B (2011) Bleaching/blinking assisted localization microscopy for superresolution imaging using standard fluorescent molecules. *Proc Natl Acad Sci* 108(52):21081–21086
- Burns DH, Callis JB, Christian GD, Davidson ER (1985) Strategies for attaining superresolution using spectroscopic data as constraints. *Appl Opt* 24(2):154–161
- Chandra T, Kirschner K, Thuret J-Y, Pope BD, Ryba T, Newman S, Ahmed K, Samarajiw SA, Salama R, Carroll T et al (2012) Independence of repressive histone marks and chromatin compaction during senescent heterochromatic layer formation. *Mol cell* 47(2):203–214
- Chen B, Gilbert LA, Cimini BA, Schnitzbauer J, Zhang W, Li G-W, Park J, Blackburn EH, Weissman JS, Qi LS et al (2013) Dynamic imaging of genomic loci in living human cells by an optimized crispr/cas system. *Cell* 155(7):1479–1491
- Chenouard N, Smal I, De Chaumont F, Maška M, Sbalzarini IF, Gong Y, Cardinale J, Carthel C, Coraluppi S, Winter M et al (2014) Objective comparison of particle tracking methods. *Nature Methods* 11(3):281
- Cosa G, Focsaneanu KS, McLean JRN, McNamee JP, Scaiano JC (2001) Photophysical properties of fluorescent dna-dyes bound to single-and double-stranded dna in aqueous buffered solution. *Photochem Photobiol* 73(6):585–599
- Cremer C, Cremer T (1978) Considerations on a laser-scanning-microscope with high resolution and depth of field. *Microsc Acta* 81:31–44
- Cremer T, Cremer C (2001) Chromosome territories, nuclear architecture and gene regulation in mammalian cells. *Nature Rev Genet* 2(4):292–301
- Cremer T, Küpper K, Dietzel S, Fakan S (2004) Higher order chromatin architecture in the cell nucleus: on the way from structure to function. *Biol Cell* 96(8):555–567
- Cremer T, Cremer M, Hübner B, Strickfaden H, Smeets D, Popken J, Sterr M, Markaki Y, Rippe K, Cremer C (2015) The 4d nucleome: Evidence for a dynamic nuclear landscape based on co-aligned active and inactive nuclear compartments. *FEBS Lett* 589:2931–2943
- Diana C, Carvalho PC (2010) Supramolecular biomimetic binding of the DNA-dye Hoechst 33258 by a synthetic macrocycle. Ph.D. thesis
- Dickson RM, Cubitt AB, Tsien RY, Moerner WE (1997) On/off blinking and switching behaviour of single molecules of green fluorescent protein. *Nature* 388(6640):355–358
- Doudna JA, Charpentier E (2014) The new frontier of genome engineering with crispr-cas9. *Science* 346(6213):1258096
- Egner A, Geisler C, Von Middendorff C, Bock H, Wenzel D, Medda R, Andresen M, Stiel AC, Jakobs S, Eggeling C et al (2007) Fluorescence nanoscopy in whole cells by asynchronous localization of photoswitching emitters. *Biophys J* 93(9):3285–3290
- Fölling J, Bossi M, Bock H, Medda R, Wurm CA, Hein B, Jakobs S, Eggeling C, Hell SW (2008) Fluorescence nanoscopy by ground-state depletion and single-molecule return. *Nature Methods* 5(11):943–945
- Früh SM, Schoen I, Ries J, Vogel V (2015) Molecular architecture of native fibronectin fibrils. *Nature Commun* 6:7275
- Grammel M, Hang HC (2013) Chemical reporters for biological discovery. *Nature Chem Biol* 9(8):475–484

- Gustafsson MGL (2000) Surpassing the lateral resolution limit by a factor of two using structured illumination microscopy. *J Microsc* 198(2):82–87
- Hagmann M, Prakash K, Best G, Kaufmann R, Birk U, Cremer C (2014) Drift correction strategies for single molecule localisation microscopy. In: Hozák P (ed) 18th international microscopy congress, number ISBN 978-80-260-6720-7
- Hagmann M, Prakash K, Cremer C (2016) Visualisation enhancement for single molecule reconstructions using wigner–seitz cells (in preparation)
- Heilemann M, Van De Linde S, Schüttelpelz M, Kasper R, Seefeldt B, Mukherjee A, Tinnefeld P, Sauer M (2008) Subdiffraction-resolution fluorescence imaging with conventional fluorescent probes. *Angew Chem Int Edition* 47(33):6172–6176
- Heintzmann R, Cremer C (1999) Laterally modulated excitation microscopy: improvement of resolution by using a diffraction grating. In: *BiOS Europe'98*. International Society for Optics and Photonics, pp 185–196
- Hell SW, Wichmann J (1994) Breaking the diffraction resolution limit by stimulated emission: stimulated-emission-depletion fluorescence microscopy. *Opt Lett* 19(11):780–782
- Hess ST, Girirajan TPK, Mason MD (2006) Ultra-high resolution imaging by fluorescence photoactivation localization microscopy. *Biophys J* 91(11):4258
- Hirschfeld T (1976) Optical microscopic observation of single small molecules. *Appl Opt* 15(12):2965–2966
- Hsu PD, Lander ES, Zhang F (2014) Development and applications of crispr-cas9 for genome engineering. *Cell* 157(6):1262–1278
- Hussels M, Brecht M (2011) Effect of glycerol and pva on the conformation of photosystem i. *Biochemistry* 50(18):3628–3637
- Jianzhuang L, Wenqing L, Yupeng T (1991) Automatic thresholding of gray-level pictures using two-dimension otsu method. In: 1991 international conference on circuits and systems, 1991. Conference proceedings, China, pp 325–327. IEEE
- Kaufmann R, Piontek J, Grüll F, Kirchgessner M, Rossa J, Wolburg H, Blasig IE, Cremer C (2012) Visualization and quantitative analysis of reconstituted tight junctions using localization microscopy. *PLoS One* 7(2):e31128
- Klein T, Löschberger A, Proppert S, Wolter S, van de Linde S, Sauer M (2011) Live-cell dstorm with snap-tag fusion proteins. *Nature Methods* 8(1):7–9
- Lemmer P, Gunkel M, Baddeley D, Kaufmann R, Urich A, Weiland Y, Reymann J, Müller P, Hausmann M, Cremer C (2008) Spdm: light microscopy with single-molecule resolution at the nanoscale. *Appl Phys B* 93(1):1–12
- Lemmer P, Gunkel M, Weiland Y, Müller P, Baddeley D, Rainer Kaufmann A, Urich HE, Amberger R, Hausmann M et al (2009) Using conventional fluorescent markers for far-field fluorescence localization nanoscopy allows resolution in the 10-nm range. *J Microsc* 235(2):163–171
- Lidke K, Rieger B, Jovin T, Heintzmann R (2005) Superresolution by localization of quantum dots using blinking statistics. *Opt Express* 13(18):7052–7062
- Manley S, Gillette JM, Patterson GH, Shroff H, Hess HF, Betzig E, Lippincott-Schwartz J (2008) High-density mapping of single-molecule trajectories with photoactivated localization microscopy. *Nature Methods* 5(2):155–157
- Miyazari Y, Ziegler-Birling C, Torres-Padilla M-E (2013) Live visualization of chromatin dynamics with fluorescent tales. *Nature Struct Mol Biol* 20(11):1321–1324
- Moerner WE, Kador L (1989) Optical detection and spectroscopy of single molecules in a solid. *Phys Rev Lett* 62(21):2535
- Müller P, Schmitt E, Jacob A, Hoheisel J, Kaufmann R, Cremer C, Hausmann M (2010) Combifish enables high precision localization microscopy as a prerequisite for nanostructure analysis of genome loci. *Int J Mol Sci* 11(10):4094–4105
- Neice A (2010) Chapter 3 - methods and limitations of subwavelength imaging. In: Hawkes PW (ed) *Advances in imaging and electron physics*, vol 163. Elsevier, pp 117–140. doi:[10.1016/S1076-5670\(10\)63003-0](https://doi.org/10.1016/S1076-5670(10)63003-0)

- Nieuwenhuizen RPJ, Lidke KA, Bates M, Puig DL, Grünwald D, Stallinga S, Rieger B (2013) Measuring image resolution in optical nanoscopy. *Nature Methods* 10(6):557–562
- Piterburg M, Panet H, Weiss A (2012) Photoconversion of dapi following uv or violet excitation can cause dapi to fluoresce with blue or cyan excitation. *J Microsc* 246(1):89–95
- Prakash K, Fournier D, Redl S, Best G, Borsos M, Tiwari VK, Tachibana-Konwalski K, Ketting RF, Parekh SH, Cremer C et al (2015) Superresolution imaging reveals structurally distinct periodic patterns of chromatin along pachytene chromosomes. *Proc Natl Acad Sci* 112(47):14635–14640
- Rao SSP, Huntley MH, Durand NC, Stamenova EK, Bochkov ID, Robinson JT, Sanborn AL, Machol I, Omer AD, Lander ES et al (2014) A 3d map of the human genome at kilobase resolution reveals principles of chromatin looping. *Cell* 159(7):1665–1680
- Rayleigh L (1896) Xv. on the theory of optical images, with special reference to the microscope. *Lond Edinb Dublin Philos Mag J Sci* 42(255):167–195
- Rust MJ, Bates M, Zhuang X (2006) Stochastic optical reconstruction microscopy (storm) provides sub-diffraction-limit image resolution. *Nature Methods* 3(10):793
- Ricci MA, Manzo C, García-Parajo MF, Lakadamyali M, Cosma MP (2015) Chromatin fibers are formed by heterogeneous groups of nucleosomes in vivo. *Cell* 160(6):1145–1158
- Schoen I, Ries J, Klotzsch E, Ewers H, Vogel V (2011) Binding-activated localization microscopy of dna structures. *Nano Lett* 11(9):4008–4011
- Sengupta P, van Engelenburg SB, Lippincott-Schwartz J (2014) Superresolution imaging of biological systems using photoactivated localization microscopy. *Chem Rev* 114(6):3189–3202
- Sheppard CJR, Wilson T (1981) Effects of high angles of convergence on $v(z)$ in the scanning acoustic microscope. *Appl Phys Lett* 38(11):858–859
- Shroff H, Galbraith CG, Galbraith JA, Betzig E (2008) Live-cell photoactivated localization microscopy of nanoscale adhesion dynamics. *Nature Methods* 5(5):417–423
- Small AR, Parthasarathy R (2014) Superresolution localization methods. *Ann Rev Phys Chem* 65:107–125
- Small A, Stahlheber S (2014) Fluorophore localization algorithms for super-resolution microscopy. *Nature Methods* 11(3):267–279
- Sunney Xie X, Dunn RC et al (1994) Probing single molecule dynamics. *Science* 265:361
- Szczurek AT, Prakash K, Lee H-K, Żurek-Biesiada DJ, Best G, Hagmann M, Dobrucki JW, Cremer C, Birk U (2014) Single molecule localization microscopy of the distribution of chromatin using hoechst and dapi fluorescent probes. *Nucleus* 5(4):331–340
- Thanisch K, Schneider K, Morbitzer R, Solovei I, Lahaye T, Bultmann S, Leonhardt H (2013) Targeting and tracing of specific dna sequences with dtales in living cells. *Nucleic Acids Res*, gkt1348
- Thompson RE, Larson DR, Webb WW (2002) Precise nanometer localization analysis for individual fluorescent probes. *Biophys J* 82(5):2775–2783
- Uno SN, Kamiya M, Yoshihara T, Sugawara K, Okabe K, Tarhan MC, Fujita H, Funatsu T, Okada Y, Tobita S et al (2014) A spontaneously blinking fluorophore based on intramolecular spirocyclization for live-cell super-resolution imaging. *Nature Chem* 6(8):681–689
- Van Oijen AM, Köhler J, Schmidt J, Müller M, Brakenhoff GJ (1998) 3-dimensional super-resolution by spectrally selective imaging. *Chem Phys Lett* 292(1):183–187
- Weiland Y, Lemmer P, Cremer C (2011) Combining fish with localisation microscopy: super-resolution imaging of nuclear genome nanostructures. *Chromosom Res* 19(1):5–23
- Whelan DR, Bell TDM (2015) Image artifacts in single molecule localization microscopy: why optimization of sample preparation protocols matters. *Sci Rep* 5:7924
- Wood AJ, Lo T-W, Zeitler B, Pickle CS, Ralston EJ, Lee AH, Amora R, Miller JC, Leung E, Meng X et al (2011) Targeted genome editing across species using zfn and talens. *Science* 333(6040):307–307
- Xu K, Zhong G, Zhuang X (2013) Actin, spectrin, and associated proteins form a periodic cytoskeletal structure in axons. *Science* 339(6118):452–456
- Zessin PJM, Finan K, Heilemann M (2012) Super-resolution fluorescence imaging of chromosomal dna. *J Struct Biol* 177(2):344–348

- Zhimulëv IF (1996) Morphology and structure of polytene chromosomes. Academic Press, New York
- Zipfel WR, Williams RM, Webb WW (2003) Nonlinear magic: multiphoton microscopy in the biosciences. *Nature Biotechnol* 21(11):1369–1377
- Żurek-Biesiada D, Szczurek AT, Prakash K, Mohana GK, Lee H-K, Roignant J-Y, Birk U, Dobrucki JW, Cremer C (2015) Localization microscopy of dna in situ using vybrant dyecycle violet fluorescent probe: a new approach to study nuclear nanostructure at single molecule resolution. *Exp Cell Res* 343:97–106
- Żurek-Biesiada D, Szczurek AT, Prakash K, Best G, Mohana GK, Lee H-K, Roignant J-Y, Dobrucki JW, Cremer C, Birk U (2016) Quantitative super-resolution localization microscopy of dna in situ using vybrant dyecycle violet fluorescent probe. *Data Brief* 7:157–171

Chromatin Architecture

Advances From High-resolution Single Molecule DNA
Imaging

Prakash, K.

2017, LIII, 152 p. 101 illus., 50 illus. in color., Hardcover

ISBN: 978-3-319-52182-4